Effective elastic and transport properties of regular honeycombs for all densities

S. Hyun and S. Torquato
Princeton Materials Institute and Department of Chemistry, Princeton University, Princeton, New Jersey 08544

(Received 3 February 2000; accepted 21 June 2000)

The effective planar elastic moduli and planar conductivity (or dielectric constant) of regular hexagonal and triangular honeycombs were investigated for the entire range of volume fractions. Only the extreme limits of the volume fraction have been studied in the past. We studied the effective properties both numerically, via finite elements, and analytically, via rigorous three-point bounds, three-point approximations, and cross-property bounds. We show here that the three-point bounds and approximations are generally in excellent agreement with the simulation data and are superior to the two-point Hashin–Shtrikman bounds. Therefore, the three-point estimates provide accurate analytical predictions of the effective properties for all densities. Both the effective bulk modulus and effective conductivity are nearly extremal in the case of hexagonal honeycombs for the entire volume-fraction range, in contrast to the effective shear modulus. In the case of triangular honeycombs, all of the property values are relatively close to being optimal. Thus, the triangular honeycomb has desirable multifunctional performance for all densities in so far as the elastic moduli, conductivity, and dielectric constant are concerned.

I. INTRODUCTION

The study of the effective mechanical, electrical, magnetic, and transport properties of cellular and other porous materials is an active area of research because of its wide applications as well as fundamental interest. However, studies have been restricted to the extreme density limits (very low and very high densities) because analytical expressions are more difficult to obtain at intermediate densities. In the low-density limit of solids, the cellular material is light weight and, with the properly designed microstructures, can possess desirable mechanical, thermal, and electrical properties.[1–3] In the high-density limit, the cellular material is characterized by a dilute concentration of cavities. However, most realistic cellular materials have densities that lie between these extreme limits.

The purpose of this paper is to quantify the effective elastic and transport behaviors of regular two-dimensional cellular materials for the entire range of densities using simulation (finite elements) and bounding techniques. Following Gibson and Ashby,[1] we refer to two-dimensional cellular materials as honeycombs, regardless of their cell shape and underlying lattice. We consider both hexagonal and triangular cells for the present study. We choose these structures because they are macroscopically isotropic and asymptotic analytic solutions are known in the extreme density limits.[1–5] Moreover, it is also known that the properties in the extreme density limits can be optimal. It is therefore of interest to determine to what extent these properties remain optimal at intermediate densities. In the intermediate-density region, the well-known Hashin–Shtrikman bounds provide analytic information on the possible range of the effective properties.[6,7] However, the Hashin–Shtrikman bounds account only for volume fraction as well as isotropy information. Bounds have been developed that incorporate more detailed information about the microstructure, such as three-point correlation functions.[8] We evaluate these so-called three-point bounds as well as recent three-point approximations[9] by determining the relevant microstructural parameters (ζ and η) using the technique of Eischen and Torquato.[10] We also use our simulation data for the effective elastic moduli to estimate the effective conductivity (or dielectric constant) by using cross-property relations.[11]

In the next section, we state rigorous bounds, three-point approximations, and asymptotic expressions for the effective properties of cellular materials. In Sec. III, we describe the finite-element technique that we use to compute the effective properties of the cellular materials as well as the microstructural parameters that arise in the three-point estimates (bounds and approximations). Section IV presents the calculated three-point parameters and the effective elastic moduli for the honeycombs for

the entire volume fraction range. Our numerical results at the extreme volume fractions are compared to the asymptotic expressions as well as the rigorous bounds. Improved bounds on the electrical conductivity for the honeycombs are obtained from the microstructural parameters and the cross-property relation. In the final section, we make concluding remarks and discuss future work.

II. HOMOGENIZATION THEORY

A. Rigorous bounds and approximations for elastic moduli and conductivity

1. Hashin–Shtrikman bounds

Consider a two-dimensional composite that consists of a solid of volume fraction ϕ and bulk and shear moduli k, G, and a void phase of volume fraction $1-\phi$. Let k_e and G_e be the effective planar bulk and shear moduli, respectively. The Hashin–Shtrikman[6,7] upper bounds on the effective moduli are given by

$$\frac{k_e}{k} \leqslant \frac{G\phi}{k(1-\phi)+G} \quad , \tag{1}$$

$$\frac{G_e}{G} \leqslant \frac{k\phi}{(k+2G)(1-\phi)+k} \quad . \tag{2}$$

The corresponding Hashin–Shtrikman upper bound on the effective electrical conductivity σ_e is given by

$$\frac{\sigma_e}{\sigma} \leqslant \frac{\phi}{2-\phi} \quad . \tag{3}$$

These are the best upper bounds on the effective elastic moduli k_e and G_e and effective conductivity σ_e given volume fraction information since they are realizable by certain microstructures.[6,7,12,13] The bounds (1)–(3) actually incorporate two-point correlation function information and hence are referred to as two-point bounds. The corresponding lower bounds on the moduli and conductivity are trivially zero. Note that because of mathematical analogy, results for the effective electrical conductivity translate immediately into equivalent results for the effective dielectric constant, thermal conductivity, and magnetic permeability.

In the low-density limit ($\phi \to 0$), the Hashin–Shtrikman bounds become

$$\frac{k_e}{k} \leqslant \frac{G}{k+G}\phi \quad , \tag{4}$$

$$\frac{G_e}{G} \leqslant \frac{1}{2}\frac{k}{k+G}\phi \quad , \tag{5}$$

$$\frac{\sigma_e}{\sigma} \leqslant \frac{\phi}{2} \quad . \tag{6}$$

We see that the effective properties are linear functions of ϕ. Similarly, in the high-density limit ($\phi \to 1$), the same bounds become

$$\frac{k_e}{k} \leqslant 1 - \frac{k+G}{G}(1-\phi) \quad , \tag{7}$$

$$\frac{G_e}{G} \leqslant 1 - 2\frac{k+G}{G}(1-\phi) \quad , \tag{8}$$

$$\frac{\sigma_e}{\sigma} \leqslant 1 - 2(1-\phi) \quad . \tag{9}$$

These asymptotic forms are linear functions of $(1-\phi)$. All isotropic cellular solids must obey the bounds (4)–(6) when $\phi \to 0$ and bounds (7)–(9) when $\phi \to 1$.

2. Three-point bounds

The sharpest three-point bounds on the effective planar bulk and shear moduli have been obtained by Gibiansky and Torquato[8] employing the variational principles. These bounds are expressed in terms of the volume fraction ϕ and certain three-point parameters ζ and η that depend on a three-point correlation function, as defined below. The three-point upper bound on the bulk modulus is given by

$$\frac{k_e}{k} \leqslant \frac{G\zeta\phi}{k(1-\phi)+G(1-\phi+\zeta\phi)} \quad , \tag{10}$$

where

$$\zeta = \frac{4}{\pi\phi(1-\phi)}\int_0^\infty \frac{dr}{r}\int_0^\infty \frac{ds}{s}\int_0^\pi d\theta\ cos(2\theta) \left[S_3(r,s,t) - \frac{S_2(r)S_2(s)}{\phi}\right] \quad . \tag{11}$$

$S_2(r)$ is two-point probability of finding the end points of a line of length r in one phase when randomly thrown into the sample. Similarly, $S_3(r,s,t)$ is three-point probability of finding the vertices of a triangle, with sides of lengths r, s, and t, in one phase. θ is the angle opposite the side of the triangle of length t. This microstructural parameter ζ lies in the closed interval [0, 1]. Note that this bound (10) coincides with the optimal Hashin–Shtrikman upper bound (1) when $\zeta = 1$.

In the case of shear modulus, the upper bound is given in terms of ζ as well as another three-point parameter η as defined by

$$\eta = \frac{16}{\pi\phi(1-\phi)}\int_0^\infty \frac{dr}{r}\int_0^\infty \frac{ds}{s}\int_0^\pi d\theta\ cos(4\theta) \left[S_3(r,s,t) - \frac{S_2(r)S_2(s)}{\phi}\right] \quad . \tag{12}$$

This microstructural parameter η also lies in the closed interval [0, 1]. For the special case of porous materials (including honeycombs), the upper bound on the shear modulus is given by

$$\frac{G_e}{G} \leqslant \frac{k\eta\phi}{[k + (1 + \eta)G](1 - \phi) + k\eta} \quad , \tag{13}$$

when $t^* \leqslant -k^{-1}$ and by

$$\frac{G_e}{G} \leqslant \frac{k\zeta\phi}{[(2 - \zeta)k + 2G](1 - \phi) + k\zeta} \quad , \tag{14}$$

when $t^* \geqslant G^{-1}$. Here t^* is a function of the three-point parameters and the elastic moduli.[8] For a two-phase composite (k_i, G_i, ζ_i, η_i; $i = 1, 2$), t^* is given by

$$t^* = \frac{\left\{\sqrt{2\zeta_1\zeta_2(k_1^{-1} - k_2^{-1})^2}(\eta_1 G_2^{-1} + \zeta_2 G_1^{-1}) - \sqrt{\eta_1\eta_2(G_1^{-1} - G_2^{-1})^2}(\zeta_1 k_2^{-1} + \zeta_2 k_1^{-1})\right\}}{\left\{\sqrt{2\zeta_1\zeta_2(k_1^{-1} - k_2^{-1})^2} + \sqrt{\eta_1\eta_2(G_1^{-1} - G_2^{-1})^2}\right\}} \quad . \tag{15}$$

For a porous material (k_1, $G_1 \to 0$, and $k_2 = k$, $G_2 = G$), this parameter t^* becomes a simple function of η, ζ, k, and G. Interestingly, these two bounds (13) and (14) are identical when $2(1 - \zeta)/\zeta = (1 - \eta)/\eta$, i.e., when t^* is finite. Note that the three-point upper bounds (13) and (14) coincide with the optimal Hashin–Shtrikman upper bound (2) when $\eta = 1$ and $\zeta = 1$, respectively.

The best upper bound on the effective conductivity using the three-point parameter ζ was derived by Milton[14] and for a porous material is given by

$$\frac{\sigma_e}{\sigma} \leqslant \frac{\phi\zeta}{1 + \zeta - \phi} \quad . \tag{16}$$

Note that it coincides with the optimal Hashin–Shtrikman upper bound (3) when $\zeta = 1$.

3. Three-point approximations

Torquato[9] developed three-point approximations for the effective elastic moduli of dispersions of inclusions in a matrix that depend on the three-point parameters ζ and η. These approximations are valid for any phase contrast for both two- and three-dimensional dispersions. For a two-dimensional sheet containing holes of arbitrary shape, the three-point approximations for k_e and G_e reduce to

$$\frac{k_e}{k} = \frac{G\phi(2\zeta - 1)}{k(1 - \phi) + G[1 + 2\phi(\zeta - 1)]} \quad , \tag{17}$$

$$\frac{G_e}{G} = \frac{k\phi(\zeta + \eta - 1)}{(k + 2G)(1 - \phi) + k[1 - \phi(2 - \zeta - \eta)]} \quad . \tag{18}$$

These expressions (17) and (18) coincide with the optimal Hashin–Shtrikman upper bounds (1) and (2) when $\eta = 1$ and $\zeta = 1$. The corresponding 3-point approximation for the effective Young's modulus E_e/E is given by

$$\frac{E_e}{E} = \frac{\phi(2\zeta - 1)(\zeta + \eta - 1)}{\{3 - 2\phi - 2(2 - \phi)(1 - \zeta) + (2 - \zeta - \eta)[2\phi(1 - \zeta) - 1]\}} \quad . \tag{19}$$

It is seen that E_e/E is independent of Poisson's ratio ν of the sheet, which we know to be exactly true for any sheet containing holes.[16,17]

B. Asymptotic behavior of elastic moduli and conductivity

1. Low-density limit

For regular honeycombs (hexagonal, triangular, square), the asymptotic forms of the effective elastic moduli and conductivity in the low-density limit are well known from standard beam theory (stretching and bending of the cell walls).[1–3] For the honeycomb with hexagonal-shaped cells, the asymptotic expressions are given by

$$\frac{k_e}{k} = \frac{G}{k + G}\phi \quad , \tag{20}$$

$$\frac{G_e}{G} = \frac{3}{2}\frac{k}{k + G}\phi^3 \quad , \tag{21}$$

$$\frac{\sigma_e}{\sigma} = \frac{\phi}{2} \quad . \tag{22}$$

The effective bulk modulus and conductivity in this limit show exactly the same linear behavior as the Hashin–Shtrikman upper bounds (4) and (6), respectively; i.e., a hexagonal honeycomb is extremal in both the effective bulk modulus and conductivity in the low-density limit. However, the asymptotic expression (21) for the effective shear modulus is much smaller than the optimal bound (5) since the former decreases as ϕ^3. This is true because a hexagonal honeycomb is much more compliant under shear loading than under hydrostatic loading due to easy bending of the walls. For the honeycomb with triangular-shaped cells, the low-density asymptotic expressions are given by

$$\frac{k_e}{k} = \frac{G}{k + G}\phi \quad , \tag{23}$$

$$\frac{G_e}{G} = \frac{1}{2}\frac{k}{k + G}\phi \quad , \tag{24}$$

$$\frac{\sigma_e}{\sigma} = \frac{\phi}{2} \quad . \tag{25}$$

Therefore, a triangular honeycomb shows both extremal bulk and shear moduli as well as extremal conductivity in this limit.

2. High-density limit

For the hexagonal honeycomb, the high-density asymptotic expressions for the effective elastic moduli and conductivity are given by

$$\frac{k_e}{k} = 1 - a\frac{k+G}{G}(1-\phi) \quad , \tag{26}$$

$$\frac{G_e}{G} = 1 - b\frac{k+G}{k}(1-\phi) \quad , \tag{27}$$

$$\frac{\sigma_e}{\sigma} = 1 - c(1-\phi) \quad . \tag{28}$$

where $a = 1.0517$, $b = 2.0825$, and $c = 2.048$b.[4,5] We see that the asymptotic expressions are very close to the Hashin–Shtrikman extremal values in this limit. The corresponding coefficients for the Hashin–Shtrikman bounds are given by $a = 1.0$, $b = 2.0$, and $c = 2.0$ [see Eqs. (7)–(9)]. However, the elastic moduli and conductivity of the triangular honeycomb in the high-density limit are somewhat lower than those of the hexagonal honeycomb since $a = 1.6152$, $b = 2.5867$, and $c = 2.5811$.[4,5]

C. Cross-property conductivity–elastic moduli bounds

For two-phase composite, Gibiansky and Torquato[11] derived cross-property bounds that relate the effective elastic moduli to the effective conductivity. In the special case of a porous solid at fixed volume fractions, the cross-property bound involving the effective bulk modulus k_e and the effective conductivity σ_e is given by

$$\sigma\left(\frac{1}{\sigma_e} - \frac{1}{\sigma_0}\right) \leqslant \frac{2kG}{k+G}\left(\frac{1}{k_e} - \frac{1}{k_0}\right) \quad , \tag{29}$$

where

$$\sigma_0 = \frac{\sigma\phi}{2-\phi} \quad , \tag{30}$$

$$k_0 = \frac{kG\phi}{k+G-k\phi} \quad , \tag{31}$$

Thus, a measurement of the effective bulk modulus k_e (effective conductivity σ_e) of a composite enables us to obtain a nontrivial bound on the effective conductivity σ_e (effective bulk modulus k_e). For example, in contrast to the aforementioned two- and three-point lower bounds on σ_e which are identically zero, relation (29) leads to a nonzero lower bound on σ_e. In low-density limit, Torquato *et al.* showed that bound (29) becomes an equality (i.e., exact) for hexagonal, triangular, and square honeycombs.

III. SIMULATION USING FINITE ELEMENT METHOD

We performed numerical simulation to study the planar effective elastic moduli and conductivity of honeycomb structures. Using the finite element method, the effective properties of regular honeycombs (hexagonal and triangular) were calculated in the wide range of volume fraction. DYNAFLOW, a finite element solver, was used for all the finite element simulations.[15] The honeycomb structures were meshed by three-node triangular finite elements. The total number of finite elements ranges from 3000 to 10000. Two dimensional elastic moduli ($k = 1.333$, $G = 1$) and conductivity ($\sigma = 1$) have been used for the elastic moduli and conductivity of the solid phase. Because of the computer memory limitation, we could not increase the resolution more, usually required in the high-density limit. Nevertheless, it has been ensured that the increase of finite elements does not change the result significantly. Figures 1 and 2 show the two different regular honeycombs at selected volume fractions. To simulate infinite systems, we only needed to consider simple unit cells with periodic boundary conditions (see Fig. 3). Uniaxial loadings and pure shear loadings have been used for the calculation of the effective stiffness tensor and conductivity tensor.

The finite element calculation provides all the local fields from which the effective properties are calculated. For the elasticity problem, the local stress σ_{ij}^n and strain ϵ_{kl}^n are provided in nth finite element. Similarly, the local current density J_i^n and electric field E_j^n are provided in nth finite element for the conductance problem. The effective properties are obtained by the homogenization method by taking the averages of these local fields.

$$k_e = \frac{(C_e)_{1111} + (C_e)_{1122}}{2} \quad , \tag{32}$$

$$G_e = (C_e)_{1212} \quad , \tag{33}$$

$$\sigma_e = (\sigma_e)_{11} \quad , \tag{34}$$

where the effective stiffness tensor $(C_e)_{ijkl}$ and effective conductivity tensor $(\sigma_e)_{ij}$ are given by

$$\langle \sigma_{ij} \rangle = (C_e)_{ijkl}\langle \varepsilon_{kl} \rangle \quad , \tag{35}$$

$$\langle J_i \rangle = (\sigma_e)_{ij}\langle E_j \rangle \quad . \tag{36}$$

Note that k_e of Eq. (32) is a plane bulk modulus. For a plane strain elasticity (applicable to oriented cylinders of any shape), $k_e = K_e + G_e/3$, where K_e is the three-dimensional bulk modulus. For a plane stress elasticity (applicable to a sheet), $k_e = 9K_eG_e/(3K_e + 4G_e)$.

Another finite element simulation was carried out to obtain the microstructural parameters ζ and η for the honeycomb structures. To do this, we employed the same technique used by Eischen and Torquato.[10] Using such microstructural information, we computed the Gibiansky–Torquato three-point estimates on the elastic moduli and conductivity (see Sec. II. A. 2). We compared the improved bounds and approximations with the simulation data as well as the two-point Hashin–Shtrikman bounds.

The effective conductivities were calculated numerically for hexagonal and triangular honeycombs in which the solid-phase conductivity $\sigma = 1$. These numerical results were compared with the rigorous bounds. The lower bound was obtained by the cross-property relation (29) incorporating with the measurement of effective bulk modulus, and the three-point upper bound (16) was obtained by the microstructural parameter ζ obtained from the simulation on the effective elastic moduli.

IV. RESULTS

A. Three-point parameters

The microstructural parameters ζ and η that we obtained numerically are presented in Fig. 4 for hexagonal and triangular honeycombs. The parameter ζ for the hexagonal honeycomb is nearly equal to unity for the entire density range. This means that the three-point upper bound (10) on k_e will provide small improvement over the optimal two-point Hashin–Shtrikman upper bound (1) for hexagonal honeycombs. By contrast, η for hexagonal honeycombs is appreciably different from unity, except in the high-density regime. Therefore, the three-point upper bounds and three-point approximations on G_e will generally provide significant improvement over the bound (2). The quantity ζ for triangular honeycombs is generally smaller than ζ for hexagonal honeycombs at fixed ϕ. Except for large ϕ, η for triangular honeycombs is larger than η for hexagonal honeycombs.

B. Effective elastic properties

In the case of the hexagonal honeycomb models, the lowest and highest values of the solid volume fraction ϕ are 0.0396 and 0.960, respectively. In the case of the triangular honeycomb models, the lowest and highest values of the solid volume fraction ϕ are 0.0681 and 0.965, respectively. At these very low and very high densities, we can use the exact asymptotic results in Sec. II. B to test our simulation results. Tables I and II summarize these comparisons. We see that the numerical results for the elastic moduli in the extreme limits show good agreement with the theoretical predictions within acceptable errors.

With reference to Fig. 5(a), it is seen that the effective bulk modulus of the hexagonal honeycomb is nearly optimal (equals the Hashin–Shtrikman upper bound) for all densities. The effective shear modulus is far from optimal for this structure for low to intermediate densities. This behavior is expected given the cubic dependence on ϕ in the asymptotic expression (21). However, the shear modulus is nearly optimal in the high-density regime. In

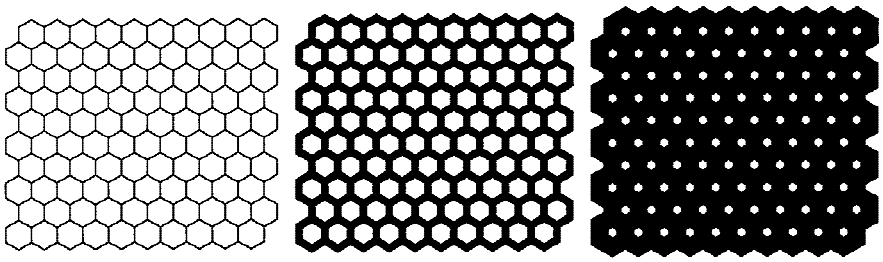

FIG. 1. Hexagonal honeycomb networks for finite element simulation with different volume fractions. Volume fractions of solid phase (black) are $\phi = 0.059$, $\phi = 0.51$, and $\phi = 0.96$, respectively. Note that the centers of the cells are the sites of a triangular lattice.

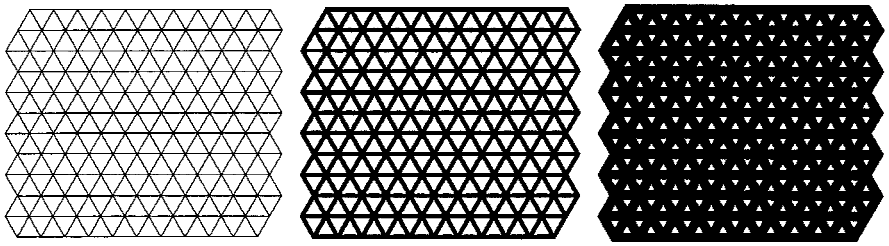

FIG. 2. Triangular honeycomb networks with different volume fractions. Volume fractions of solid phase (black) are $\phi = 0.061$, $\phi = 0.50$, and $\phi = 0.95$, respectively. Note that the centers of the cells are the sites of a hexagonal lattice (also called a "honeycomb" lattice).

the case of the triangular honeycomb, both the effective bulk and shear moduli are relatively close to optimal behavior, as shown in Fig. 6.

We present the improved three-point bounds in Fig. 5 and 6, which are determined from the microstructural parameters ζ and η. Upper bounds on the bulk moduli are given by (10) for both hexagonal and triangular honeycombs. However, upper bounds on the shear moduli are given by either of two expressions (13) and (14), depending on the parameter t^*. For the hexagonal honeycomb, the upper bound on the effective shear modulus is given by (13) for $0 \leqslant \phi \leqslant 0.72$ and by (14) for $0.72 \leqslant 1$. However, in the range $0.72 \leqslant \phi \leqslant 1$, the bounds (13) and (14) are virtually identical and hence one can use upper bound (13) for all volume fractions for the hexagonal honeycomb. For the triangular honeycomb, the upper bound on the effective shear modulus is given by Eq. (14) for all volume fractions. These upper bounds on the elastic moduli are compared with the numerical results in the figures. The two-point Hashin–Shtrikman bounds are also included. Note that the new three-point bounds provide significant improvement in the intermediate density region, except in the case of the shear modulus of the hexagonal honeycomb in the low-density limit.

The three-point approximations (17) and (18) for the elastic moduli are also presented in Figs. 5 and 6. Note that these approximate estimations show excellent agreement with the numerical data, especially for the shear modulus of the hexagonal honeycomb in the low-density limit. It is superior to the three-point bound, as shown in Fig. 5(b). In Table III, we summarize the best three-point estimations (bounds and approximations) on the effective

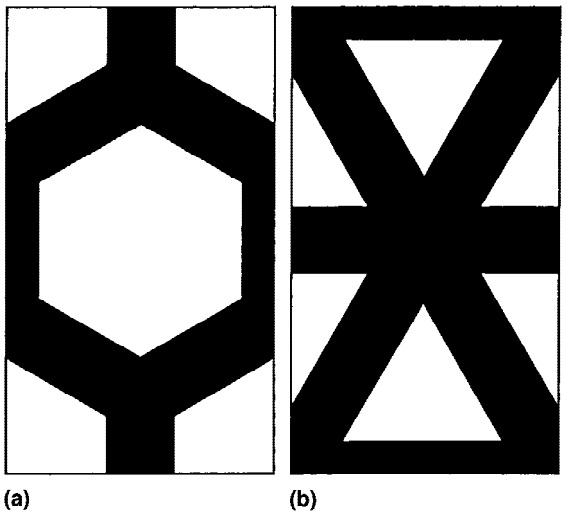

FIG. 3. Unit cells of (a) hexagonal honeycomb and (b) triangular honeycomb for the finite element simulation.

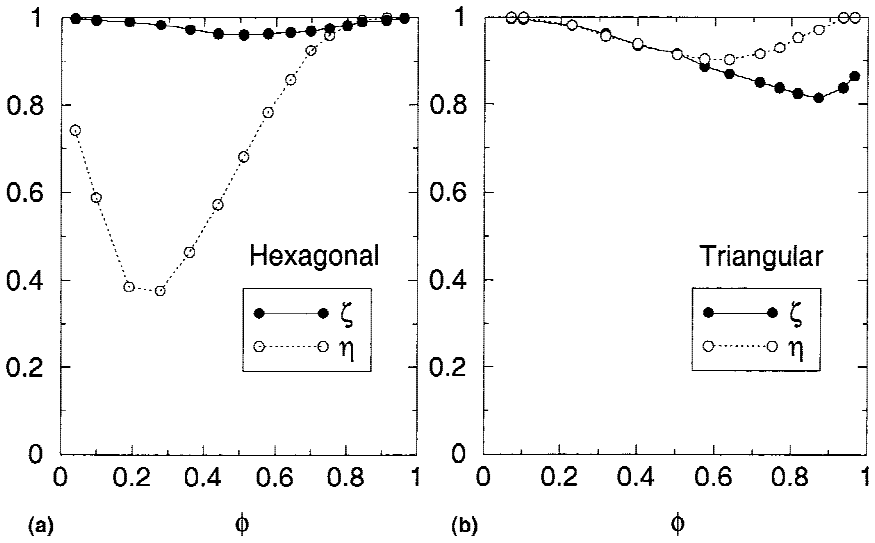

FIG. 4. (a) Microstructural parameters ζ and η for the hexagonal honeycomb versus the volume fraction ϕ. (b) Same parameters for the triangular honeycomb.

TABLE I. Scaled effective bulk modulus and shear modulus in the extreme density limits for the hexagonal honeycomb.

	k_e/k		G_e/G	
ϕ	Theory	Simulation	Theory	Simulation
0.0396	0.0170	0.0173	5.32×10^{-5}	6.49×10^{-5}
0.960	0.926	0.909	0.854	0.872

TABLE II. Scaled effective bulk modulus and shear modulus in the extreme density limits for the triangular honeycombs.

	k^e/k		G_e/G	
ϕ	Theory	Simulation	Theory	Simulation
0.0681	0.0292	0.0301	0.0195	0.0201
0.965	0.868	0.889	0.842	0.868

properties for the honeycomb structures. The three-point bounds and approximations are nearly indistinguishable from one another except for the shear modulus of the hexagonal honeycomb.

In Fig. 7, we present the simulated Young's moduli for the honeycombs, in which Poisson's ratio $\nu = 0.1429$, and the corresponding three-point approximation (19). However, as noted earlier, the simulated Young's moduli should be independent of Poisson's ratio.[16,17] This property has been numerically verified at some selected volume fractions for both honeycomb structures for several different Poisson's ratios ($\nu = 0.1429$, 0.3333, 0.5000). All of the simulated Young's moduli E_e/E for these Poisson's ratios are identical up to at least three significant figures, and therefore, these data are indistinguishable on the scale of Fig. 7. This further attests to the accuracy of our numerical results.

C. Effective conductivity

Numerical results for the effective conductivities of the honeycombs and corresponding rigorous bounds are presented in Fig. 8. The lower bound is given by the cross-property conductivity–elastic moduli relation (29), and the upper bound is given by (16) in terms of the microstructural parameter ζ. Note that the gap between the upper and lower bounds becomes significantly narrow for both hexagonal and triangular honeycombs. The

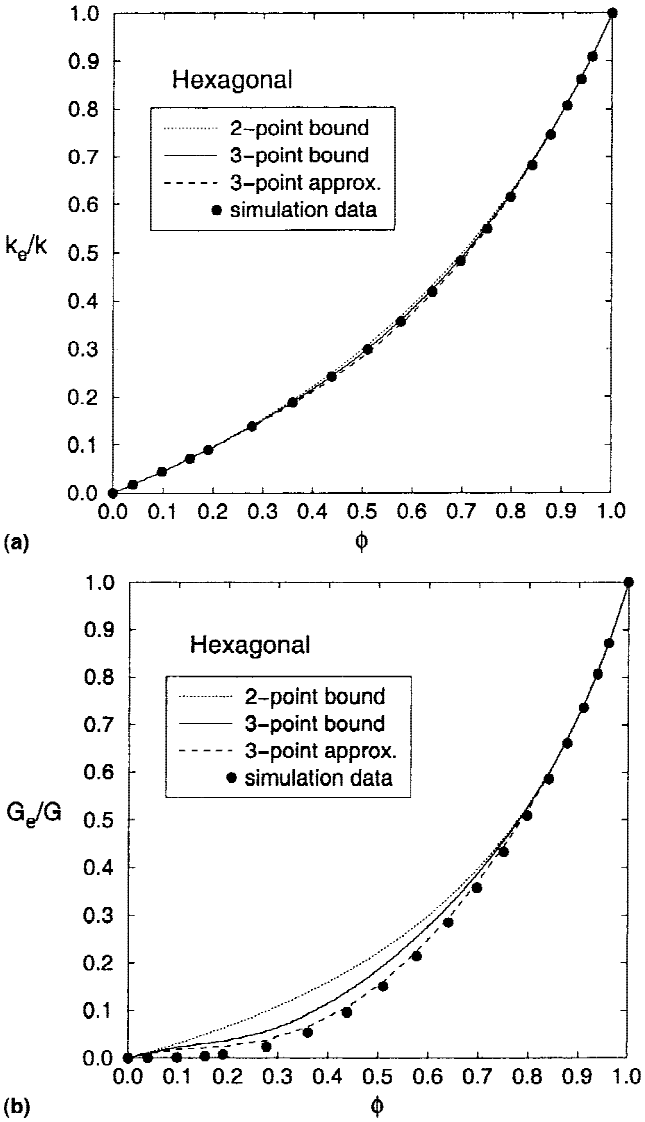

FIG. 5. (a) Effective bulk modulus and (b) shear modulus for hexagonal honeycombs versus volume fraction of the solid phase (ϕ). Simulation data are compared to 2- and 3-point upper bounds as well as 3-point approximations.

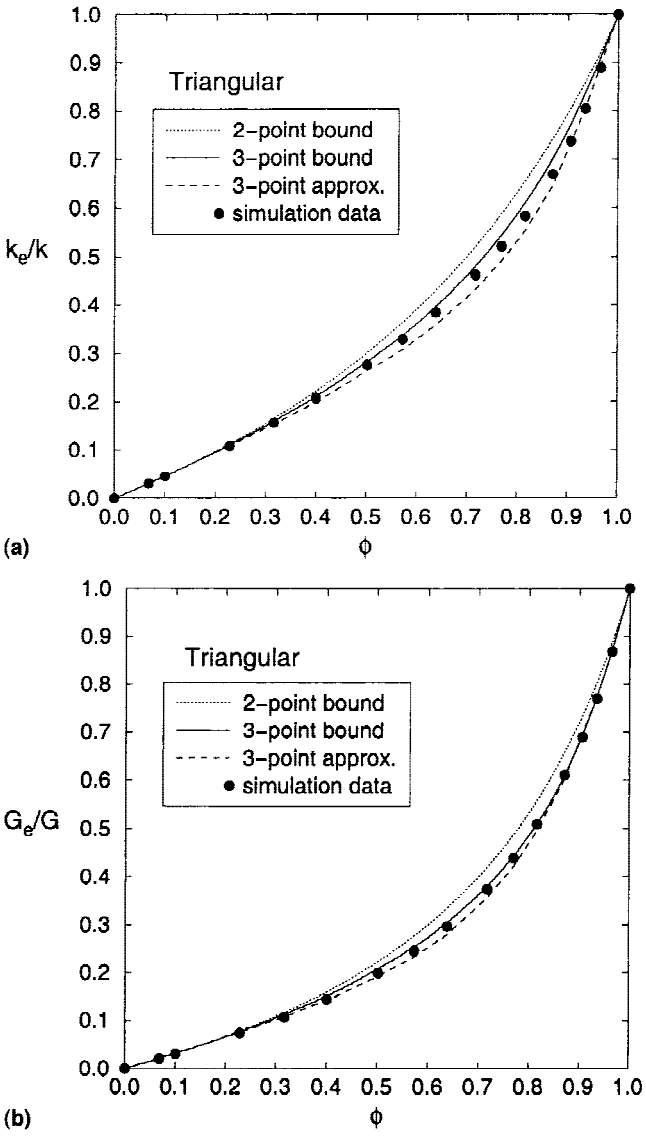

FIG. 6. (a) Effective bulk modulus and (b) shear modulus for triangular honeycombs versus volume fraction of the solid phase (ϕ). Simulation data are compared to 2- and 3-point upper bounds as well as 3-point approximations.

cross-property lower bound obviously provides significant improvement over the two- and three-point bounds that are trivially zero.

TABLE III. Best three-point estimations on the effective properties of honeycombs.

Property	Hexagonal cells	Triangular cells
k_e	Bound (10) or approximation (17)	Bound (10) or approximation (17)
G_e	Approximation (18)	Bound (14) or approximation (18)
σ_e	Bound (16)	Bound (16)

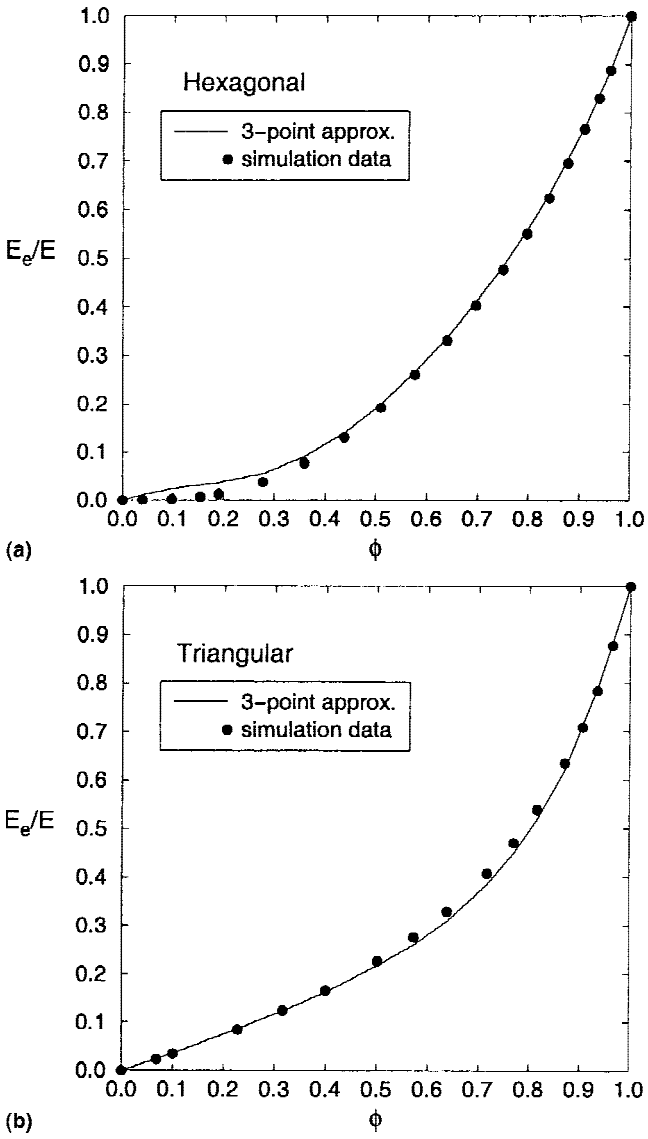

FIG. 7. Effective Young's modulus versus volume fraction of the solid phase (ϕ) for (a) hexagonal honeycomb and (b) triangular honeycomb. All data are obtained for $\nu = 0.1429$. Simulation results are compared to Torquato's 3-point approximations.

V. CONCLUDING REMARKS AND DISCUSSION

In this paper, we have computed the planar effective elastic and transport properties for hexagonal and triangular honeycomb structures over the entire range of volume fractions via finite elements. Thus, for densities in between the extreme density limits, we have determined the elastic moduli where analytical estimates are not available. Both the effective bulk modulus and effective conductivity are nearly extremal in the case of hexagonal honeycombs for the entire volume-fraction range. In the case of triangular honeycombs, all of the properties are relatively close to the corresponding optimal value.

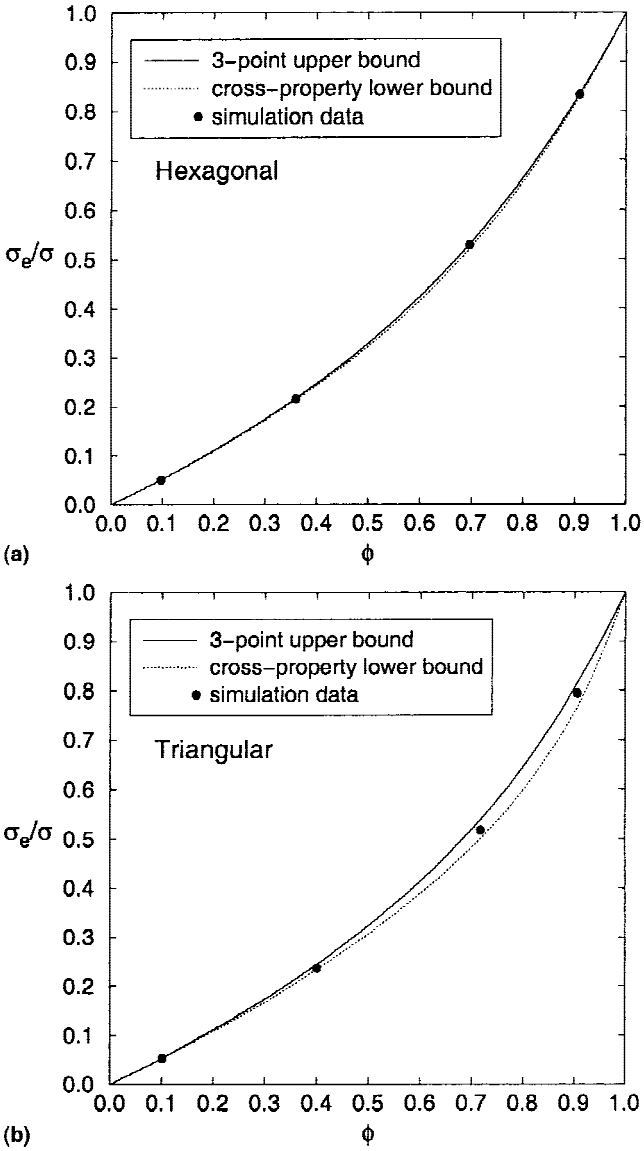

FIG. 8. The effective conductivities of (a) hexagonal and (b) triangular honeycombs obtained by the finite element calculation are plotted with respect to the volume fraction of solid phase. The simulation results are compared with the lower bound from cross-property relations of conductivity and elastic moduli and the three-point upper bound obtained using the microstructural parameter ζ.

Therefore, triangular honeycombs are desirable multifunctional cellular materials for all densities in so far as the elastic moduli, conductivity, and dielectric constant are concerned.

We also have computed improved three-point bounds and approximations for the effective elastic moduli and the three-point bounds for the effective conductivity obtained by evaluating the microstructural parameter ζ and η for the honeycomb structures. The three-point estimates of the effective properties, given in Sec. II, are generally in excellent agreement with the simulation data for all densities and thus provide accurate analytical expressions for the properties of the honeycombs. The three-point estimates are generally superior to the two-point Hashin–Shtrikman bounds. We have also shown that the cross-property relation provides a significantly improved lower bound on the effective conductivity of honeycombs.

In light of the above, it is natural to ask whether there exist cell shapes that are truly optimal at intermediate densities. This question has been partially answered in the case of the bulk modulus by Vigdergauz.[18,19] He found the optimal shape of a hole in a square lattice of such holes. There are no published results for the optimal shape of a hole on other lattices such that the effective bulk modulus is maximized. Moreover, for the effective shear modulus, very little is known about the optimal hole shape for any lattice structure. Torquato *et al.* conjectured that one may be able to find optimal hole shapes on the sites of a hexagonal lattice that maximize the effective bulk and shear moduli and effective conductivity.[3] Employing an inverse topology optimization technique, Sigmund found lattice structures that are close to being optimal for the effective bulk and shear moduli at a single value of the volume fraction.[20] We are currently using numerical topology optimization techniques to address these questions concerning optimal hole shapes for a variety of lattices at all volume fractions.[21]

ACKNOWLEDGMENT

We gratefully acknowledge the support of the Office of Naval Research under Grant No. N00014-96-1-1028.

REFERENCES

1. L.J. Gibson and M. Ashby, *Cellular Solids* (Pergamon Press, New York, 1988).
2. R.M. Christensen, Z. Angew. Math. Phys. **46,** S506 (1995).
3. S. Torquato, L.V. Gibiansky, M.J. Silva, and L.J. Gibson, Int. J. Mech. Sci. **40,** 71 (1998).
4. I. Jasiuk, J. Chen, and M.F. Thorpe, Appl. Mech. Rev. **47,** S18 (1994).
5. M.F. Thorpe, Proc. R. Soc. London, Ser. A **437,** 215 (1992).
6. Z. Hashin and S. Shtrikman, J. Mech. Phy. Solids **11,** 127 (1963).
7. Z. Hashin, J. Mech. Phys. Solids **13,** 119 (1965).
8. L.V. Gibiansky and S. Torquato, J. Mech. Phys. Solids **43,** 1587 (1995).
9. S. Torquato, J. Mech. Phys. Solids **46,** 1411 (1998).
10. J.W. Eischen and S. Torquato, J. Appl. Phys. **74,** 159 (1993).
11. L.V. Gibiansky and S. Torquato, Phys. Rev. Lett. **71,** 2927 (1993).
12. K.A. Lurie and A.V. Cherkaev, J. Opt. Theor. Appl. **46,** 571 (1985).
13. G.A. Francfort and F. Murat, Arch. Ration. Mech. Anal. **94,** 307 (1986).
14. G.W. Milton, J. Mech. Phys. Solids **30,** 177 (1982).
15. J.H. Prevost, DYNAFLOW version 99 finite element solver (1999).
16. A.R. Day, K.A. Snyder, E.J. Garboczi, and M.F. Thorpe, J. Mech. Phys. Solids **40,** 1031 (1992).
17. A.V. Cherkaev, K.A. Lurie, and G.W. Milton, Proc. R. Soc. London, Ser. A **438,** 519 (1992).
18. S.B. Vigdergauz, Mech. Solids **24,** 57 (1989).
19. S.B. Vigdergauz, J. Appl. Mech. **3,** 300 (1994).
20. O. Sigmund, J. Mech. Phys. Solids **48,** 397 (1999).
21. S. Hyun and S. Torquato (unpublished).